11-15-2002

Photoacoustic Study of KrF Laser Heating of Si: Implications for Laser Particle Removal

Sergey I. Kudryashov
Florida State University

Susan D. Allen
Florida State University, allens17@erau.edu

Photoacoustic study of KrF laser heating of Si: Implications for laser particle removal

Sergey I. Kudryashov[a)]
Department of Chemistry and Biochemistry, Florida State University, Tallahassee, Florida 32306-4390

Susan D. Allen[b)]
Department of Chemistry and Biochemistry, Florida State University, Tallahassee, Florida 32306 and Department of Electrical and Computer Engineering, FAMU-FSU College of Engineering, Tallahassee, Florida 32306-4390

(Received 3 May 2002; accepted 8 July 2002)

A photoacoustic study of KrF laser heating of Si has revealed that the dominant mechanism of acoustic generation is thermoacoustic with a considerable contribution from the concentration–deformation mechanism at laser fluences below the Si melting threshold of 0.5 J/cm^2. Upon Si melting the contraction of the molten material contributes significantly to acoustic generation. At fluences above 1.4 J/cm^2 laser ablation of the molten layer enhances the amplitude of the compression pulse and diminishes that of the rarefaction pulse. The results of photoacoustic measurements allow optimization of experimental conditions for dry laser particle removal. © *2002 American Institute of Physics.* [DOI: 10.1063/1.1503859]

I. INTRODUCTION

Dry laser cleaning (DLC) is a well-known technique for micron and sub-micron particle removal from critical surfaces, e.g., semiconductor devices, lithography masks[1–4] and high density memory devices.[5] Although DLC is frequently described as resulting from the pure thermal ''trampoline''[1] or ''hopping'' effects[6] occurring during thermal expansion of a nanosecond laser-heated substrate or an absorbing particle, respectively, a variety of optical, thermal, acoustic, mechanical, thermochemical and mass transport phenomena are generally involved in the DLC process[2–4] and detailed understanding of DLC mechanisms is still lacking.

Photoacoustic (PA) spectroscopy, photodeflection (PD) spectroscopy, and infrared (IR) radiometry are recognized methods for the study of photothermal phenomena in condensed matter.[7,8] In the particular case of DLC, PD techniques have been used to study the vibrational response of a Si surface upon visible laser irradiation, exhibiting the unipolar temporal vibrational velocity profile characteristic of thermal expansion.[3] Nevertheless, depending on the experimental conditions of laser–matter interaction (laser intensity, wavelength, and pulse width, material properties such as optical absorption, ambipolar diffusion, and the thermal diffusivity), more complicated expansion/contraction cycles of a laser-excited semiconductor surface layer, e.g., Si contraction preceding its expansion at 1064 nm laser wavelength excitation due to electron–hole plasma (EHP) excitation,[9–12] may be observed as bipolar or multipolar vibrational velocity transients,[9–13] all of which can strongly affect the DLC efficiency and can make particle removal dynamics much more complicated.[4] Although a general analysis of the vibrational surface response for laser-heated materials (including semiconductors) is available,[8] its application to the optimization of experimental conditions of DLC has not been reported, especially for DLC with excimer lasers, which are widely used for this application.

In this work the vibrational response and basic acoustic generation mechanisms were studied for clean and dry Si wafers heated by a KrF laser using a ''direct'' contact variant of PA spectroscopy with detection of acoustic transients at the rear side of the sample under study.[8]

II. EXPERIMENT

The beam of a 248 nm, 20 ns KrF excimer laser (Lambda Physik, LPX 210) was apertured in its central part by a 1 cm wide vertical slit and was focused ($f=8$ cm) on a 0.25 mm thick Si(100) wafer at normal incidence. The laser beam has nearly rectangular and Gaussian fluence distributions in the horizontal (X) and vertical (Y) directions (see insets in Fig. 2) with characteristic dimensions of $x=5$ and $\sigma_y^{1/e}=1.5$ mm, respectively. Laser energy [0.2 J/pulse ($\pm 3\%$) after the aperture] was attenuated by calibrated color filters (Corning Glass Works) and was measured for each pulse by splitting off a part of the beam to a pyroelectric detector (Gentec ED-500).

Photoacoustic studies were done with the Si wafer attached to the front surface of a fast 1.5 mm thick, 8 mm wide acoustic transducer (PZT ceramic, effective bandwidth of 3–30 MHz, 3 mm protective brass disk) by means of a thin layer of vacuum grease, providing acoustic contact between the wafer and transducer. The relatively large laser spot on the wafer surface provided PA measurements of a vibrational velocity in the near acoustic field ($Z/Z_{\mathrm{diffr}}\approx 0.1$), where the characteristic diffraction length, $Z_{\mathrm{diffr}}\approx \pi x\sigma_y/4Z_{\mathrm{ac}}\approx 30$ mm, and the distance Z_{ac} that sound travels during the laser pulse τ(full width half

a) Permanent address: Institute for High Energy Densities, Joint Institute of High Temperatures, 127412 Moscow, Russia; electronic mail: sergeikudryashov@hotmail.com, sergeikudryashov@chat.ru
b) Author to whom correspondence should be addressed; electronic mail: sdallen@mailer.fsu.edu

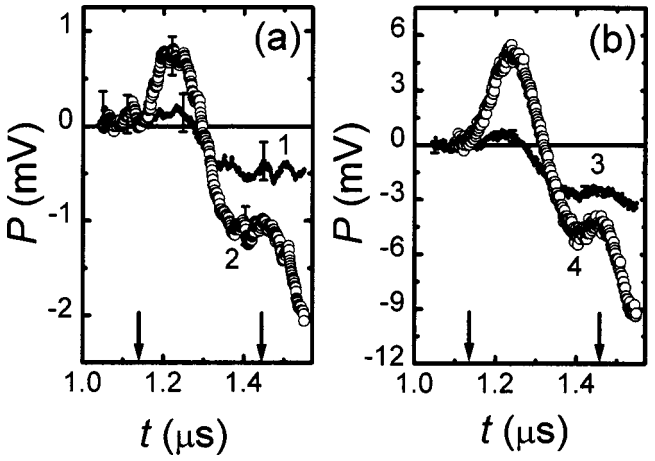

FIG. 1. Experimental PA transients at different laser fluences: (a) 0.18 (1) and 0.44 J/cm^2 (2), (b) 0.67 (3) and 2.5 J/cm^2 (4). The arrows show the operational time window for the acoustic transducer determined by echoes and the PA signal delay in the acoustic delay line.

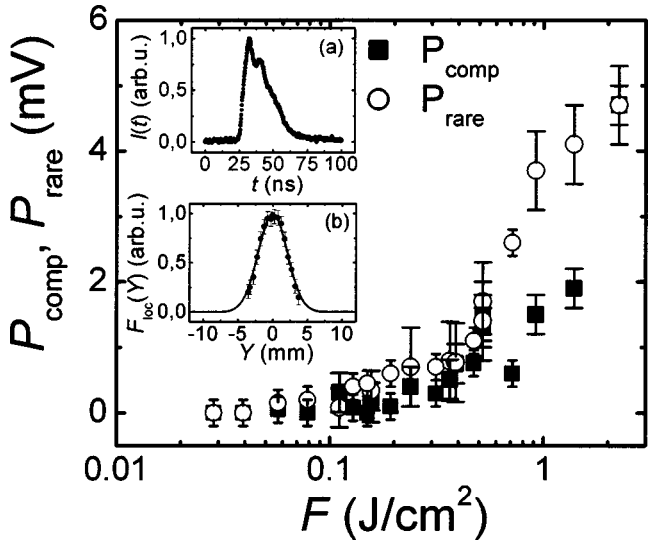

FIG. 2. P_{comp} and P_{rare} values as a function of laser fluence F. Insets: (a) temporal intensity profile of the KrF laser measured with a fast photodiode, (b) Gaussian distribution of F_{loc} in the Y direction. (Note that P_{comp} and P_{rare} points overlap at $F=2.5$ J/cm^2).

maximum)$\approx$20 ns, is equal to about 0.2 mm for the Si longitudinal acoustic velocity $C_l[100]\approx 8.4\times 10^3$ m/s.[14] A LeCroy 9360 storage oscilloscope triggered by a fast silicon photodiode was used to simultaneously record PA transients delayed by 1.1 μs due to the protective brass disk and to measure laser pulse energy using the photodiode. The excimer laser was triggered manually in a single-shot mode by a pulse generator (Stanford Research Systems DG 535). Inspection of irradiated spots was made with an optical microscope (Mitutoyo WH).

Typical PA transients, representing temporal profiles of acoustic pressure $P(t)$ [or vibrational (interface) velocity, $\nu_{\mathrm{vib}}(t)$] for different regimes of acoustic excitation at the free boundary of the Si wafer for a laser fluence F of 0.027–2.5 J/cm^2, are presented in Fig. 1. Within the operating time window of the acoustic transducer (the first 300 ns) these transients exhibit prominent bipolar wave forms where the first, compression (positive) pulse corresponds to expansion of a laser-excited near-surface region of the Si wafer and the second, rarefaction (negative) pulse corresponds to contraction in the region resulting from cooling at the end of the laser pulse.[8] The bipolar profile of the PA wave forms recorded is characteristic for the thermoacoustic regime of acoustic generation at a free air/Si boundary,[8] but its asymmetry over the whole fluence range shows pronounced influence of other acoustic generation mechanisms known for Si, i.e., the nonthermal concentration–deformation mechanism (contraction of Si due to a laser-induced EHP),[8–12] melting [contraction $\theta_m=(\Delta V/V_0)_m$],[10–11,13] and laser ablation at higher fluences when Si damage occurs.[15] Broadening of the wave forms by 3–4 times and diminution of their amplitudes occur because of dissipative losses of $\sim$20 dB in the 3 mm protective brass disk (specific acoustic absorption coefficient of brass at a frequency of about 10 MHz equal to $\alpha_{\mathrm{ac}}/f\approx 7\times 10^{-6}$ Hz^{-1} m^{-1})[14] and reflections at all interfaces in the acoustic delay line.

For the nanosecond laser pulse width in this work an acoustic generation regime on a free Si surface is quasistatic due to the acoustically ''thin'' energy deposition depth $L_{\mathrm{dep}}/C_l\tau\ll 1$ for $L_{\mathrm{dep}}\approx\max\{\alpha^{-1}, L_D\approx(D\tau_R)^{1/2}, L_T\approx(\chi\tau)^{1/2}, L_m\}$, where α, D, L_D, τ_R, χ, L_T, and L_m are the optical absorption coefficient at 248 nm, EHP ambipolar diffusivity, diffusion length and characteristic recombination time, thermal diffusivity and thermal diffusion length for solid Si, and melt depth, respectively. In this regime PA transient pressure $P(t)$ follows the time derivative of the sum of the weighted deformation stress, $\sigma_D=-\delta N_{\mathrm{eh}}$, and temperature-induced stress, $\sigma_T=+K\beta(T)(T-300)$, in the laser-excited near-surface layer of Si,[8] including contributions from the tensile stress upon melting, $\sigma_m=-|K\theta_m|$, and recoil ablative pressure, $P_{\mathrm{abl}}(t)$, where K is the bulk modulus of solid Si, δ is the deformation potential, $\beta(T)$ is the strongly temperature-dependent thermal expansion coefficient, and N_{eh} is the EHP density, according to the expression

$$P(t)\approx\frac{1}{C_l}\frac{d(\sigma_D L_D+\sigma_T L_T+\sigma_m L_m)}{dt}+P_{\mathrm{abl}}(t). \tag{1}$$

To consider quantitative changes in the vibrational velocity of the PA compression and rarefaction pulses, which are proportional to the corresponding acoustic pressures P_{comp} and P_{rare} (Fig. 2), their amplitudes were multiplied by factors of about 1.25 and 1.1, respectively, to account for the diffraction effect in the acoustic near field for $Z/Z_{\mathrm{diffr}}\approx 0.1$.[8] It should be noted that the correction factors may differ significantly near the characteristic thresholds (melting, ablation) because the surface size of the molten or ablated region, i.e., the size of the corresponding acoustic source, is very small at laser fluences just slightly above these thresholds.

An iterative deconvolution procedure was applied to the diffraction corrected fluence dependencies of $P_{\mathrm{comp}}(F)$ and $P_{\mathrm{rare}}(F)$ to take into account the averaging of P_{comp} and P_{rare} values over the Gaussian laser fluence distribution (Fig. 2 inset) in the Y direction at the maximum fluence F

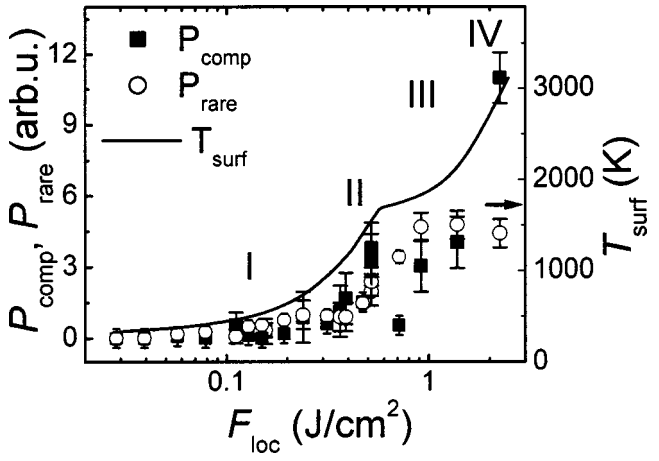

FIG. 3. Diffraction corrected and spatially deconvoluted P_{comp} and P_{rare} values as a function of local laser fluence F_{loc} showing the characteristic regions I–IV (left axis); maximum surface temperature of Si as a function of laser fluence F (right axis). The Si melt temperature is marked with an arrow on the right axis.

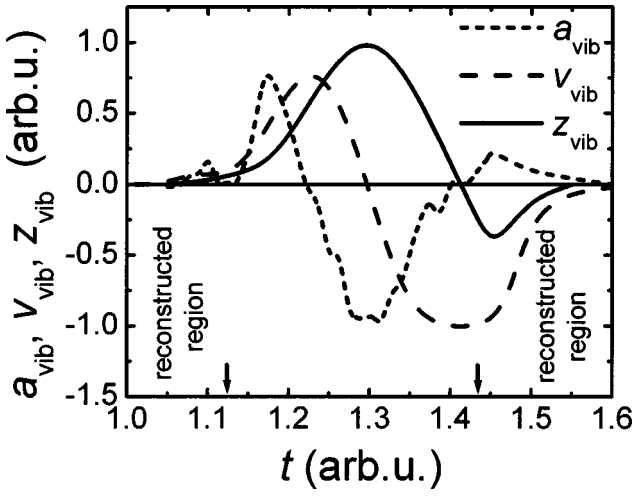

FIG. 4. Qualitative temporal behavior of acceleration a_{vib}, vibrational velocity ν_{vib}, and displacement z_{vib}, of a laser-excited Si surface calculated by integrating and differentiating an experimental vibrational velocity transient at a fluence of 0.44 J/cm^2 (below the Si melting threshold) extrapolated beyond the acoustic transducer operational time window marked with arrows.

$$P(F)=\frac{\int_0^F P(F_{loc})W(F_{loc},F)dF_{loc}}{\int_0^F W(F_{loc},F)dF_{loc}}, \tag{2}$$

$$\int_{F_1}^{F_2} W(F_{loc},F)dF_{loc}=\mathrm{erf}(Y_2)-\mathrm{erf}(Y_1),$$

$$\int_0^F W(F_{loc},F)dF_{loc}=\mathrm{erf}(\infty)=1. \tag{3}$$

The contributions to the total P_{comp} or P_{rare} values from spots with different local fluences, F_{loc}, have different statistical weights $W(F_{loc},F)$, determined by the error function for the Gaussian fluence distribution. Starting from the P value at the minimum $F=F_{loc}$, each next P value at higher F is calculated using the already known values at lower fluences, thus replacing both integrals in expression (2) with the corresponding sums.

III. RESULTS AND DISCUSSION

Several distinct features are observed in the resultant $P_{comp}(F_{loc})$ and $P_{rare}(F_{loc})$ curves (Fig. 3): (1) monotonic, nearly linear increase of P_{comp} and P_{rare} values at $F_{loc}<0.4$ J/cm^2 (region I), (2) a sharp rise of P_{comp} and P_{rare} at 0.4–0.5 J/cm^2 (region II), followed by (3) a dip of P_{comp} and a simultaneous increase of P_{rare} in the range of 0.5–1.4 J/cm^2 (region III). Finally, a sharp rise in P_{comp} takes place at a nearly constant P_{rare} for $F_{loc}>1.4$ J/cm^2 in region IV, corresponding to a visible spark and damage to the Si surface.

In region I, there is a quasilinear growth of P_{comp} and P_{rare} with increasing F_{loc} consistent with literature data for both IR and ultraviolet (UV) nanosecond laser heating experiments.[9–13] The relatively low vibrational response in this region results predominantly from the nonlinear dependence of thermal and deformation stresses on temperature and EHP density, resulting in high L_{dep} values at moderate temperatures (due to the thermal conductivity κ of Si scaling as $\kappa\sim T^{-1}$) and at moderate EHP densities (due to longer lifetimes and diffusion times for EHP at lower plasma densities) and thus effectively decreasing these temperature- and plasma-dependent weighted stresses (see the numerical estimates of these parameters below). The contributions of thermoacoustic and concentration–deformation mechanisms seem to be comparable, producing the asymmetrical bipolar wave form of PA transients with lower expansion velocities and higher contraction velocities [cf. Figs. 1(a), 2 and 3] due to the considerable negative contribution of the concentration–deformation mechanism. This effect of EHP may also be illustrated by the acceleration $a_{vib}(t)$ and displacement $z_{vib}(t)$ transients in Fig. 4 calculated by differentiating and integrating, respectively, the experimental vibrational velocity $\nu_{vib}(t)$ transient at a laser fluence of 0.44 J/cm^2 with the assumption of the absence of any acoustic signal before the arrival of the laser-generated acoustic pulse at the transducer at 1.15 μs and rapidly decreasing $\nu_{vib}(t)$ after $t\geqslant 1.45$ μs. Vibrational wave forms outside of this transducer operational time window were reconstructed using the above assumptions as shown in Fig. 4. The bipolar shape of the Si surface vibrational velocity response at low fluences, $F_{loc}<0.5$ J/cm^2, is apparent, as is the additional small minimum of $z_{vib}(t)$ and maximum of $a_{vib}(t)$, resulting from the significant concentration–deformation contribution in this fluence range. This behavior differs from the unipolar $\nu_{vib}(t)$ and the corresponding step-like $z_{vib}(t)$ and bipolar $a_{vib}(t)$ profiles obtained from photodeflection studies measured on the same time scale with a visible laser pump pulse,[3] but are very typical for the Si vibrational velocity response with expansion/contraction and contraction/expansion cycles in UV and IR spectral ranges,[9–12] respectively, illustrating the need for introduction of the concentration–deformation contraction effect into the one-dimensional thermal expansion model previously used to describe DLC of Si.[3,4] Considering the poor DLC efficiency in region I, the relatively low vibrational response of Si in this fluence range does not provide, apparently, optimal condi-

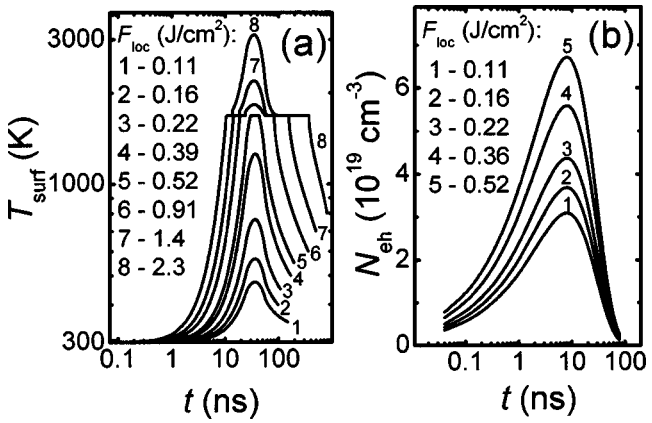

FIG. 5. Calculated transients of Si surface temperature (a) and EHP density (b) shown in order of increasing fluence. The plateau in (a) corresponds to the Si melt temperature, 1689 K.

tions for cleaning applications, but further PA experiments with higher temporal resolution during the pump laser pulse would be desirable.

At $0.4<F_{\rm loc}<0.5$ J/cm^2 (region II) the nonlinearity of the Si thermal conductivity and EHP lifetimes/diffusion times on temperature and plasma density, respectively, reduces $L_{\rm dep}$ values considerably, resulting in a sharp rise of both $P_{\rm comp}$ and $P_{\rm rare}$ values (Fig. 3), while maintaining the asymmetric bipolar wave form of the PA transients [Fig. 1(a), curve 2]. As the vibrational velocity strongly increases in this fluence range, this regime of Si laser heating, obviously, would be most important for DLC of Si surfaces.

In region III, a simultaneous decrease of $P_{\rm comp}$ and a sharp increase of $P_{\rm rare}$ appearing as the strongly asymmetric wave forms [Fig. 1(b), curve 3] seems to result, as shown elsewhere,[10–11,13] from Si surface melting and consequent Si contraction, $\theta_m \approx 10\%$, at fluences of 0.5–0.75 J/cm^2 for the 248 nm wavelength and a laser pulse width of about 20 ns.[16] The interface vibrational velocity during the acceleration stage, which is approximately proportional to $P_{\rm comp}$, remains nearly constant over the range of 0.5–1.4 J/cm^2, while that at the deceleration stage is significantly enhanced by contraction of the material during melting. Nevertheless, this regime of Si laser heating is not of practical interest as Si melting is normally highly undesirable in DLC applications.

The laser ablation threshold of Si at 248 nm is 1.3–1.5 J/cm^2,[15] where the boiling point of Si ($T_{\rm boil} \approx 3.6\times10^3$ K)[14] is assumed to be achieved. It is not unexpected that we observe at fluences $F_{\rm loc}>1.4$ J/cm^2 (region IV), that the $P_{\rm comp}$ value exceeds that of $P_{\rm rare}$ due to the additional compression recoil pressure of ablated products (Fig. 3). In this region a visible spark appeared on the Si surface during laser irradiation and a shallow crater was observed on inspection of the Si wafers with an optical microscope after multiple-shot exposure.

Maximum temperature at the Si wafer surface $T_{\rm surf}$ and its transients were calculated as a function of laser fluence $F_{\rm loc}$ using a high-order implicit scheme "SLIM"[17] to solve the nonsteady-state thermal conduction equation with temperature-dependent parameters of the Si solid and liquid phases [Figs. 3 and 5(a)]. The temperature dependence of the thermal conductivity of solid Si was taken as $1.58\times10^3 T^{-1.23}$ W/cm K,[18] while the heat capacity, optical reflectivity R, and absorption coefficient at 248 nm were assumed to be constant (1.99 J/cm^3 K, 0.6, 1.65×10^6 cm^{-1} for the solid and 2.4 J/cm^3 K, 0.68, 1.8×10^6 cm^{-1} for the liquid phases of Si, respectively).[18,19] In contrast to similar calculations in the visible wavelength (indirect band gap) region, the optical properties of Si in the ultraviolet (direct band gap) region are not strong functions of temperature. These approximate calculations give reasonable estimates of the surface temperatures for the onset of Si melting ($T_m=1689$ K,[14] region III) and ablation ($T_{\rm boil}\approx 3.6\times10^3$ K,[14] region IV) consistent with the observed behavior of $P_{\rm comp}(F_{\rm loc})$ and $P_{\rm rare}\times(F_{\rm loc})$ curves shown in Fig. 3. The close agreement of the experimental and calculated melting thresholds ($\sim$0.5 J/cm^2) is probably a fortuitous result of counterbalanced temperature dependencies of the optical and thermal properties of solid Si near its melting point that were not included in these calculations.

Finally, the relative contributions of thermoacoustic, deformation, melting, and ablative mechanisms of acoustic generation were analyzed in regions I–IV and the corresponding vibrational velocities $\nu_{\rm vib}(t)$ were estimated. In region I, the total internal stress is $\sigma=\sigma_D+\sigma_T$ [cf. Eq. (1)]. In order to evaluate the deformation stress $\sigma_D=-\delta N_{\rm eh}$, estimates of a EHP density have been made at different laser intensities $I_{\rm loc}(t)$ with a laser radiation quantum $\hbar\omega$ according to the expression[8]

$$N_{\rm eh}(t)\approx\frac{(1-R)I_{\rm loc}(t)\tau_R}{\hbar\omega L_D}, \tag{4}$$

where τ_R is the EHP characteristic recombination time and L_D is the EHP diffusion length, assuming an efficient Auger recombination process with $\gamma\approx4\times10^{-31}$ cm^6/s and negligible rate constants (10^2cm/s and 10^7 Hz) for surface and radiative recombination for polished Si wafers.[8,20] When $\tau_R\approx(\gamma N_{eh}^2)^{-1}$ and $L_D\approx(D\tau_R)^{1/2}$ are substituted in this expression, one can obtain a self-consistent expression for the time-dependent quasistationary N_{eh} value

$$N_{\rm eh}(t)\approx\sqrt{\frac{(1-R)I_{\rm loc}(t)}{\hbar\omega\sqrt{D\gamma}}}. \tag{5}$$

At laser fluences of 0.1–0.5 J/cm^2 and a fixed EHP diffusivity value $D\approx20$ cm^2/s,[20] typical EHP and thermal parameter values are: $\tau_R\sim10^{-9}-10^{-8}$ s, $L_{\rm dep}\approx L_D\sim1-5$ μm$\geqslant L_T\sim1-2$ μm, $N_{\rm eh}\sim10$ cm^{-3},[19,20] $\Delta T=(T-300)\sim10^2-10^3$ K [cf. Figs. 3, 5, and 6(a)]. Using the Si bulk modulus $K\approx10^{11}$ Pa, thermal expansion coefficient $\beta\sim4\times10^{-6}$ K^{-1} and deformation potential $\delta=8$ eV, respectively,[8,14] comparable magnitudes of the weighted thermoacoustic and deformation stresses, $\sigma^*_{T,D}=\sigma_{T,D}\times L_{T,D}/C_l\tau$, are obtained ($10^5-10^6$ Pa over the fluence range). The estimates given in Fig. 6(b) are qualitatively consistent with the experimentally measured PA amplitudes (Figs. 2–3) reproducing the increase of the thermoacoustic contribution at $F_{\rm loc}>0.3$ J/cm^2. The estimated weighted deformation stress, σ^*_D, seems to be nearly constant over a wide fluence range, in agreement with $P_{\rm rare}$ behavior in Figs. 2–3, because L_D and σ_D values scale

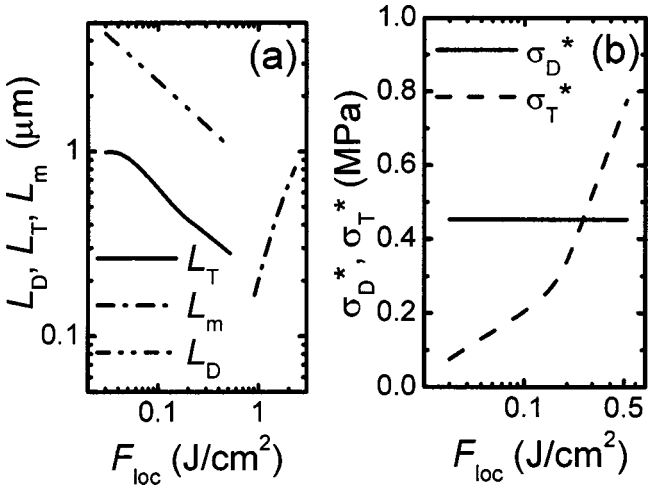

FIG. 6. (a) Calculated EHP diffusion length L_D, thermal diffusion length L_T, and melt depth L_m of solid Si as a function of laser fluence below (for L_D and L_T values) and above (for L_m) the Si melting threshold, respectively. (b) Estimated absolute values of weighted deformation, $\sigma_D^*=\sigma_D \times L_D/C_l\tau$, and thermoacoustic $\sigma_T^*=\sigma_T\times L_T/C_l\tau$ stresses as a function of laser fluence below the Si melt threshold.

as $N_{\rm eh}^{-1}$ and $N_{\rm eh}$, respectively [cf. Eq. (1)]. Estimates for transient PA pressure and vibrational velocity yield $P(t) \sim \sigma(t)L_{\rm dep}/C_l t \sim 10^5-10^6$ Pa and $\nu_{\rm vib}(t)\sim P(t)/\rho C_l \sim 0.01-0.1$ m/s, respectively, for the solid Si mass density ρ equal to 2.3 g/cm^3,[14] in good qualitative agreement with results of previous photodeflection measurements of Si vibrational velocity.[3]

In the fluence range of 0.5–1.4 J/cm^2 (region III) there is an additional contribution to the PA signal from Si contraction upon melting, $-|K\theta_m|(dL_m/C_l dt)$, decreasing $P_{\rm comp}$ and increasing $P_{\rm rare}$ values, which is equal, on average, to $(P_{\rm rare}-P_{\rm comp})/(P_{\rm rare}+P_{\rm comp})\approx 30\%-40\%$ (Fig. 3), assuming constant thermoacoustic and deformation contributions over the fluence range. According to our calculations using the SLIM code and typical thermophysical parameters of Si,[14] the melt front propagates 100–800 nm into the Si bulk during the excimer laser pulse in this fluence range [Fig. 6(a)]. Estimating a melt front velocity value of 10 m/s and assuming constant thermoacoustic and deformation contributions to σ during Si melting on the order of the maximum σ value in region I (10^8 Pa), one can find comparable values of $P(t)$ components due to the thermoacoustic effect and melting, both 10^6-10^7 Pa, i.e., nearly 1 order of magnitude higher than $P(t)$ values in region I, in agreement with the experimental data in Figs. 1–3.

The transient ablative recoil pressure $P_{abl}(t)$ has been estimated at $F_{\rm loc}\approx 2.5$ J/cm^2 (region IV) significantly above the ablation threshold of 1.3–1.5 J/cm^2,[15] taking the positive difference between $P_{\rm comp}$ and $P_{\rm rare}$ at this fluence (more exactly, approximately half of $P_{\rm comp}-P_{\rm rare}$) as a result of positive ablative contribution to both $P_{\rm comp}$ and $P_{\rm rare}$ (Fig. 3). Taking into account the rapid rise of $P_{\rm comp}$ at this fluence value and previous $P(t)$ estimates in region III, an estimate of $P_{abl}(t)$ amplitude yields about 10^7 Pa. Although laser ablation has a high acoustic efficiency, the removal rate is low, resulting in a shallow crater even after exposure to tens of laser pulses.

IV. CONCLUSIONS

In conclusion, the basic mechanisms of acoustic generation in Si heated with 20 ns KrF laser radiation, namely, thermoacoustic and deformation mechanisms as well as melting and ablation, have been studied. The photoacoustic transients had bipolar temporal profiles exhibiting multicycle acceleration/deceleration dynamics of the air/Si interface. The optimal laser fluence for dry laser cleaning of critical Si surfaces, corresponding to a relatively high vibrational response of Si, has been determined to be close to the Si melting threshold of 0.5 J/cm^2.

[1] A. C. Tam, W. P. Leung, W. Zapka, and W. Ziemlich, J. Appl. Phys. **71**, 3515 (1992).
[2] X. Wu, E. Sacher, and M. Meunier, J. Appl. Phys. **87**, 3618 (2000).
[3] M. Mosbacher *et al.*, in *Particles on Surfaces 7*, edited by K. L. Mittal (VSP, 2001).
[4] N. Arnold, G. Schrems, T. Muehlberger, M. Bertsch, M. Mosbacher, P. Leiderer, and D. Baeuerle, Proc. SPIE **4426**, 340 (2002).
[5] Y. F. Lu, W. D. Song, M. H. Hong, B. S. Teo, T. C. Chong, and T. S. Low, J. Appl. Phys. **80**, 499 (1996).
[6] J. D. Kelley, M. I. Stuff, F. E. Hovis, and G. J. Linford, Proc. SPIE **1415**, 211 (1991).
[7] *Photothermal Investigation of Solids and Liquids*, edited by J. A. Sell (Academic, San Diego, CA, 1989), Chaps. 1–3.
[8] V. E. Gusev and A. A. Karabutov, *Laser Optoacoustics* (AIP, New York, 1993), Chaps. 2–4,7.
[9] W. B. Gustler and D. H. Habing, Phys. Rev. Lett. **18**, 1058 (1967).
[10] N. Baltzer, M. von Allmen, and M. W. Sigrist, Appl. Phys. Lett. **43**, 826 (1983).
[11] I. A. Veslovskiy, B. M. Zhiryakov, A. I. Korotchenko, and A. A. Samokhin, Kvant. Elektron. (Moscow) **12**, 381 (1985) [Sov. J. Quantum Electron. **15**, 246 (1985)].
[12] S. M. Avanesyan, V. E. Gusev, and N. I. Zheludev, Appl. Phys. A: Mater. Sci. Process. **40**, 163 (1986).
[13] G. Gorodetsky, J. Kanicki, T. Kazyaka, and R. L. Melcher, Appl. Phys. Lett. **46**, 547 (1985).
[14] I. S. Grigor'ev and E. Z. Meilikhov, *Fizicheskie Velichini* (Physical Quantities, Energoatomizdat, Moscow, 1991) (in Russian).
[15] W. P. Leung and A. C. Tam, Appl. Phys. Lett. **60**, 23 (1992); Y. F. Lu, M. H. Hong, and T. S. Low, J. Appl. Phys. **85**, 2899 (1999).
[16] J. Narayan, C. W. White, M. J. Aziz, B. Strizker, and A. Walthius, J. Appl. Phys. **57**, 564 (1985); G. E. Jellison, Jr., D. H. Lowndes, D. N. Mashburn, and R. F. Wood, Phys. Rev. B **34**, 2407 (1986); R. Tsu, D. Lubben, T. R. Bramblett, and J. E. Greene, J. Vac. Sci. Technol. A **9**, 223 (1991); X. Xu, C. P. Grigoropoulos, and R. E. Russo, Appl. Phys. Lett. **65**, 1745 (1994).
[17] R. Singh and J. Viatella, computer code SLIM, University of Florida (1991, 1992).
[18] J. Narayan, R. B. James, O. W. Holland, and M. J. Aziz, J. Vac. Sci. Technol. A **3**, 183 (1985).
[19] *Handbook of Optical Constants of Solids*, edited by E. D. Palik (Academic, Orlando, FL, 1985); K. M. Shvarev, B. A. Baum, and P. V. Gel'd, Fiz. Tverd. Tela (Leningrad) **16**, 3246 (1974) [Sov. Phys. Solid State **16**, 2111 (1975)]; K. D. Li and P. M. Fauchet, Appl. Phys. Lett. **51**, 1747 (1987).
[20] M. I. Gallant and H. M. van Driel, Phys. Rev. B **26**, 2133 (1982); J. F. Young and H. M. van Driel, *ibid.* **26**, 2147 (1982).